

Spatial resolution study and power calibration of the high- k scattering system on NSTX^{a)}

W. Lee,^{1,b)} H. K. Park,¹ M. H. Cho,¹ W. Namkung,¹ D. R. Smith,² C. W. Domier,³ and N. C. Luhmann, Jr.

¹Department of Physics, POSTECH, Pohang 790-784, Republic of Korea

²Princeton Plasma Physics Laboratory, Princeton, New Jersey 08543, USA

³Department of Applied Science, University of California at Davis, Davis, California 95616, USA

(Presented 13 May 2008; received 12 May 2008; accepted 21 July 2008; published online 31 October 2008)

NSTX high- k scattering system has been extensively utilized in studying the microturbulence and coherent waves. An absolute calibration of the scattering system was performed employing a new millimeter-wave source and calibrated attenuators. One of the key parameters essential for the calibration of the multichannel scattering system is the interaction length. This interaction length is significantly different from the conventional one due to the curvature and magnetic shear effect.

© 2008 American Institute of Physics. [DOI: 10.1063/1.2969404]

I. INTRODUCTION

Anomalous electron transport induced by short scale turbulence is one of the important issues in tokamak plasmas. Since the ion transport driven by the long wavelength turbulence is well understood and often suppressed to the neoclassical level by geometrical and $E \times B$ shear effects in NSTX,¹ NSTX plasma, which has a large electron gyroradius, is well suited for electron thermal transport studies. Many theoretical studies²⁻⁶ have been published on anomalous electron thermal transport driven by the electron thermal gradient instability. Experimental studies in various devices such as DIII-D,⁷ Tore-Supra,^{2,8,9} and FT-2¹⁰ have been performed, and experiments on NSTX plasma can extend the study beyond the previous studies.

The multichannel (five) collective scattering system based on 1 mm (280 GHz) has been installed on NSTX to measure the electron gyroscale fluctuation.¹¹ The five-channel detection system was designed to measure the frequency spectra of density fluctuations at five discrete wavenumbers. The range of wavenumber spans up to $k_{\perp} \leq 20 \text{ cm}^{-1}$ which corresponds to $k_{\perp} \rho_e \leq 0.7$. The wavenumber resolution is typically $\Delta k_{\perp} \sim 0.7 \text{ cm}^{-1}$ which is based on a probe beam waist of $\sim 3 \text{ cm}$. Probe and scattered beams are nearly on the midplane so that the detected fluctuations are primarily radial or perpendicular to the magnetic surface. In data analysis, small components in poloidal and toroidal directions are also considered. Steerable launching and receiving optics have been used to control the position of the scattering volume ranging from the magnetic axis to the plasma outer edge.

In order to achieve relative and absolute calibration of the scattered power, it is important to quantify the interaction

length for each wavenumber. The interaction length in various magnetic field configurations was investigated to identify the effects of nonuniform magnetic field on the spatial resolution of the scattering experiment. Since the plasma turbulence is anisotropic in general with $k_{\perp} \geq k_{\parallel}$, where the subscripts \perp and \parallel represent the perpendicular and the parallel components to the magnetic field, respectively, the variation of the magnetic field direction within the scattering volume can modify the detecting efficiency of the receiver owing to the varying momentum matching condition. The previous studies¹²⁻¹⁴ employed instrumental selectivity $F(r) = \exp(-\{2k \sin[\xi(r)/2]/\Delta\}^2)$ in calculation of the scattering resolution, where $\xi(r)$ is the change in pitch angles of magnetic field lines and Δ is the wavenumber resolution. In this paper, the scattering resolution is calculated with the k -matching function defined in Eq. (3) for several magnetic field configurations.

II. STUDY OF SPATIAL RESOLUTION OF THE SCATTERING EXPERIMENT

A. Basic scattering principle

The scattering process is the three-wave coupling among electromagnetic waves—incident and scattered waves and a plasma density fluctuation wave. During the scattering process, energy and the momentum have to be conserved as $\omega_s = \omega_i + \omega$ and $\vec{k}_s = \vec{k}_i + \vec{k}$, where the subscripts s and i refer to the scattered and the incident wave, respectively. Since the frequency of the probe and scattered beam is significantly higher than that of the plasma waves, the momentum matching condition yields the Bragg relationship

$$\vec{k} = 2\vec{k}_i \sin\left(\frac{\theta_s}{2}\right), \quad (1)$$

where θ_s is the scattering angle. The scattered power due to a coherent density fluctuation^{15,16} is

^{a)} Contributed paper, published as part of the Proceedings of the 17th Topical Conference on High-Temperature Plasma Diagnostics, Albuquerque, New Mexico, May 2008.

^{b)} Electronic mail: wooschang@pppl.gov.

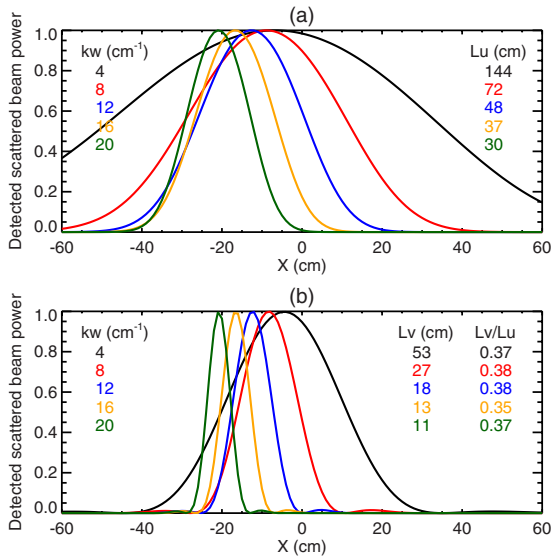


FIG. 1. (Color online) Interaction length in (a) uniform magnetic field and (b) the toroidal field curvature with $\vec{k}_w = \vec{k}_r$, where \vec{k}_r is the radial component. L_u and L_v represent the interaction lengths in uniform field and the toroidal curvature, respectively.

$$P_s(\vec{r}) = \frac{1}{4} P_0 \tilde{n}_e^2 r_e^2 \lambda_i^2 L_v^2 f(\vec{k}_w, \vec{k}_m), \quad (2)$$

where P_0 is the probe beam power, \tilde{n} is the density fluctuation, $r_e = e^2 / 4\pi\epsilon_0 m_e c^2$ is the classical electron radius, λ_i is the probe beam wavelength, and L_v is the interaction length. The k -matching function $f(\vec{k}_w, \vec{k}_m)$ is defined as

$$f(\vec{k}_w, \vec{k}_m) = \exp\left[-2 \frac{(\vec{k}_w - \vec{k}_m)_\perp^2}{(2/a)^2}\right] \text{sinc}^2\left[\frac{(\vec{k}_w - \vec{k}_m)_\parallel}{2/L}\right], \quad (3)$$

where \vec{k}_w is the fluctuation wave vector, $\vec{k}_m = \vec{k}_s - \vec{k}_i$ is the matched wave vector, a is the probe beam radius, and L is the longitudinal scattering volume.

B. Interaction length L_v in three magnetic field configurations

Nonuniform magnetic field effect on the longitudinal spatial resolution in the scattering experiment is numerically investigated. At first, the interaction length (defined as $1/e^2$

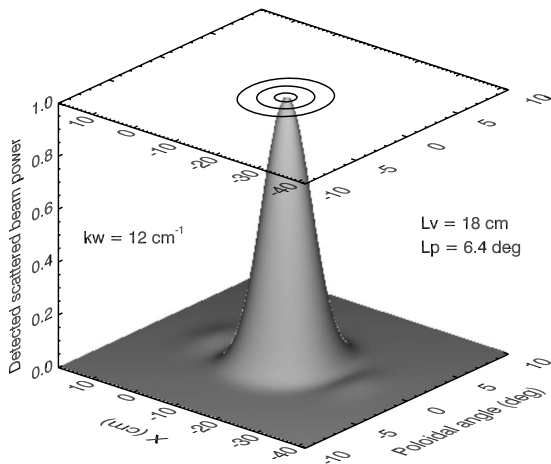


FIG. 2. Interaction length in the toroidal curvature considering poloidal component; $\vec{k}_w = \vec{k}_r + \vec{k}_p$ and $k_w = 12 \text{ cm}^{-1}$.

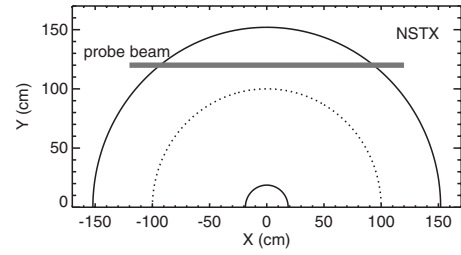


FIG. 3. Gaussian beam propagation on the equatorial midplane of NSTX like machine with $y = 120 \text{ cm}$.

width of the detected scattered beam power along the probe beam) in uniform magnetic field is calculated as a reference, as shown in Fig. 1(a).

Second, since the fluctuation wave propagates perpendicularly to the local magnetic field line, the toroidal field curvature reduces the region which satisfies the Bragg relation within the scattering volume. The calculated result with $\vec{k}_w = \vec{k}_r$ (radial component) is shown in Fig. 1(b) and the interaction lengths are reduced to 40% compared to those of the uniform case. The interaction length considering the poloidal component k_p in addition to the radial component k_r is shown in Fig. 2. Here the receiver was aligned for k_r detection. The half $1/e^2$ width on the poloidal angle is about 3.2 deg and it corresponds to $k_p/k_r \sim 0.06$, i.e., the receiver is poloidally well localized.

Third, NSTX-like machine geometry (Fig. 3) is used in calculation of the magnetic shear effect on the interaction length. The fluctuation wave vector is assumed to be $\vec{k}_w = \vec{k}_r + \vec{k}_\theta$, where \vec{k}_θ is the component in the electron diamagnetic direction $\hat{k}_\theta = \nabla p \times \hat{B}$ on the flux surface and has both poloidal and toroidal components as $\vec{k}_\theta = \vec{k}_p + \vec{k}_r$. The magnetic field employed in this calculation is based on the result of an equilibrium code (EFIT) calculation of the shot number 124882 at 0.4 s. The pitch angle of magnetic field lines and calculated interaction lengths are shown in Fig. 4. The calculated interaction lengths are pretty close to those from the toroidal curvature case without magnetic shear because the shear effect is relatively small due to the poloidally narrow detectable angle as shown earlier.

These calculations will be experimentally verified using an acoustic cell¹⁷ which can excite acoustic waves with a known frequency, wavenumber, and well defined direction of the propagation. The uniform and toroidal curvature cases

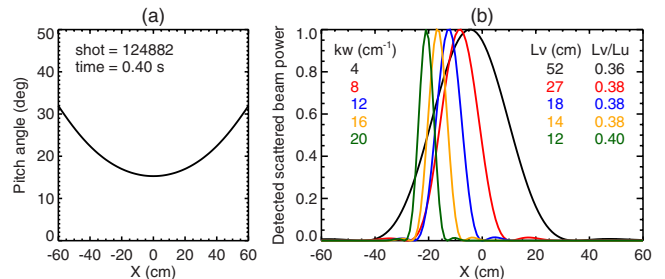


FIG. 4. (Color online) (a) Pitch angle of magnetic field lines and (b) the calculated interaction length in NSTX-like magnetic shear geometry with $\vec{k}_w = \vec{k}_r + \vec{k}_\theta$ and $k_\theta/k_r = 0.2$, where \vec{k}_θ is the component in the electron diamagnetic direction.

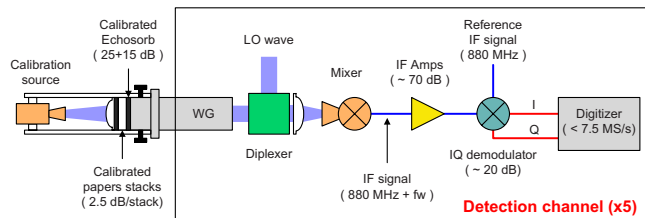


FIG. 5. (Color online) Experimental setup for the power calibration for one channel of the five-channel heterodyne receiver.

are straightforward: the acoustic cell has a fixed angle in uniform case and can be pointed to the radial direction along the probe beam path in the toroidal curvature case. However, the magnetic shear case needs a complicated three dimensional alignment of the acoustic cell angle at each probe beam path. The desired wavenumbers can be obtained by changing the driving frequency of the acoustic cell knowing the acoustic speed in a given material. The acoustic speed of TPX (transparent plastic for visible and ~ 1 mm waves) is 2.2×10^5 cm/s.

III. POWER CALIBRATION

The power calibration of the high- k scattering system has been carried out with a variable frequency millimeter wave source to find out the power response of the five-channel heterodyne receiver system. A diagram of the experimental setup is shown in Fig. 5. The calibration source power is -4 dBm ($=0.4$ mW) and it was attenuated to -54 , -49 , and -47 dBm by the optical attenuators (combination of the calibrated paper stacks and standard Echosorb). The output spectral power is the time averaged $10 \log(V^2(f)/R)$, where $V(f)$ is the Fourier transform of $V(t)_{\text{out}}$. Figure 6 shows the measured power response of the receivers. Here the power response decibels is defined as output spectral power (dBm)–input power (dBm). The difference in response among the channels comes from various factors such as coupling efficiency to the mixer, transmission line, and amplifier gain. Since the detection system is sensitive to the polarization of the scattered power, the polarization of the calibration source wave has been optimized for each channel.

ACKNOWLEDGMENTS

The authors would like to thank E. Mazzucato, R. Kaita, and L. Guttadora for physical and technical contributions to this work. This work was supported by the U.S. Department

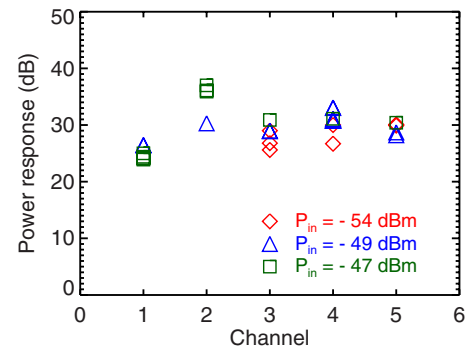


FIG. 6. (Color online) Measured power response. The difference in the response among channels is mainly due to the difference in the coupling efficiency to the mixer and the amplifier gain. The maximum value in each channel is most correct.

of Energy Contract Nos. DE-AC02-76CH03073 and DE-FG02-99ER54518, and Department of physics at POSTECH.

- ¹S. M. Kaye, R. E. Bell, D. Gates, B. P. LeBlanc, F. M. Levinton, J. E. Menard, D. Mueller, G. Rewoldt, S. A. Sabbagh, W. Wang, and H. Yuh, *Phys. Rev. Lett.* **98**, 175002 (2007).
- ²W. Horton, P. Zhu, G. T. Hoang, T. Aniel, M. Ottaviani, and X. Garbet, *Phys. Plasmas* **7**, 1494 (2000).
- ³W. Dorland, F. Jenko, M. Kotschenreuther, and B. N. Rogers, *Phys. Rev. Lett.* **85**, 5579 (2000).
- ⁴F. Jenko and W. Dorland, *Phys. Rev. Lett.* **89**, 225001 (2002).
- ⁵W. M. Nevins, J. Candy, S. Cowley, T. Dannert, A. Dimits, W. Dorland, C. Estrada-Mila, G. W. Hammett, F. Jenko, M. J. Peuschel, and D. E. Shumaker, *Phys. Plasmas* **13**, 122306 (2006).
- ⁶R. E. Waltz, J. Candy, and M. Fahey, *Phys. Plasmas* **14**, 056116 (2007).
- ⁷T. L. Rhodes, W. A. Peebles, X. Nguyen, M. A. Van Zeeland, J. S. de-Grassie, E. J. Doyle, G. Wang, and L. Zeng, *Rev. Sci. Instrum.* **77**, 10E922 (2006).
- ⁸G. T. Hoang, W. Horton, C. Bourdelle, B. Hu, X. Garbet, and M. Ottaviani, *Phys. Plasmas* **10**, 405 (2003).
- ⁹W. Horton, G. T. Hoang, C. Bourdelle, B. Hu, X. Garbet, M. Ottaviani, and L. Golas, *Phys. Plasmas* **11**, 2600 (2004).
- ¹⁰E. Z. Gusakov, A. D. Gurchenko, A. B. Altukhov, V. V. Bulanin, L. A. Esipov, M. Yu Kantor, D. V. Kouprienko, S. I. Lashkul, A. V. Petrov, and A. Yu Stepanov, *Plasma Phys. Controlled Fusion* **48**, B443 (2006).
- ¹¹D. R. Smith, E. Mazzucato, T. Musat, H. Park, D. Johnson, L. Lin, C. W. Domier, M. Johnson, and N. C. Luhmann, *Rev. Sci. Instrum.* **75**, 3840 (2004).
- ¹²P. Devynck, X. Garbet, C. Laviron, J. Payan, S. K. Saha, F. Gervais, P. Hennequin, and A. Quemeneur, *Plasma Phys. Controlled Fusion* **35**, 63 (1993).
- ¹³E. Mazzucato, *Phys. Plasmas* **10**, 753 (2003).
- ¹⁴E. Mazzucato, *Plasma Phys. Controlled Fusion* **48**, 1749 (2006).
- ¹⁵H. Park, Ph.D. thesis, University of California Los Angeles, 1984.
- ¹⁶J. Sheffield, *Plasma Scattering of Electromagnetic Radiation* (Academic, New York, 1975).
- ¹⁷H. Park, C. X. Yu, W. A. Peebles, N. C. Luhmann, Jr., and R. Savage, *Rev. Sci. Instrum.* **53**, 1535 (1982).